Biosensors and Bioelectronics 126 (2019) 558–564

Contents lists available at ScienceDirect

Biosensors and Bioelectronics

journal homepage: www.elsevier.com/locate/bios

A novel ECL sensor based on a boronate affinity molecular imprinting technique and functionalized SiO_2@CQDs/AuNPs/MPBA nanocomposites for sensitive determination of alpha-fetoprotein

Guichun Mo, Xinxin He, Chunqin Zhou, Dongmei Ya, Jinsu Feng, Chunhe Yu, Biyang Deng*

Key Laboratory for the Chemistry and Molecular Engineering of Medicinal Resources (Ministry of Education of China), School of Chemistry and Pharmaceutical Sciences, Guangxi Normal University, Guilin 541004 China

ARTICLE INFO

Keywords:
Alpha-fetoprotein
Boronate-affinity
ECL sensor
Molecular imprinting
Carbon quantum dots

ABSTRACT

In this work, a boronate-affinity sandwich electrochemiluminescence (ECL) sensor was constructed to detect alpha-fetoprotein (AFP) based on a multiple signal amplification strategy. Gold nanoparticles (AuNPs) were utilized and modified on the surface with chitosan in order to facilitate electron transfer. The composite of the molecularly imprinted polymer (MIP) enhanced the selectivity of alpha-fetoprotein detection. 4-mercaptophenylboronic acid (MPBA) was used as the tracing tag for capture of alpha-fetoprotein. SiO_2 nanoparticles carried carbon quantum dots (CQDs) labeled with gold nanoparticles and produced an ECL signal. Under the optimum experimental conditions, the linear range for alpha-fetoprotein was between 0.001 and 1000 ng/mL with a correlation coefficient of 0.9952, and the detection limit was 0.0004 ng/mL (S/N = 3). This proposed ECL sensor displayed several advantages, including outstanding selectivity, fine reproducibility, high sensitivity, low detection limit and wide linear range. Furthermore, the newly constructed boronate-affinity sandwich ECL sensor was successfully applied to the determination of alpha-fetoprotein in serum samples, indicating great potential for application in clinical diagnostics.

1. Introduction

Protein glycosylation is one of the general and multitudinous protein decorations in which complex glycans are affiliated to glycoproteins. Glycoproteins play key roles in many biological processes, such as inter- and intra-cellular signaling, molecular recognition, and immune response (Hart and Copeland, 2010; Rudd et al., 2001). In addition, a great number of glycoproteins are used as therapeutic targets and disease biomarkers (Li et al., 2013). As an oncogenic glycoprotein, alpha-fetoprotein (AFP) is a 'molecular signature' of the physiological state in adults and is constantly employed as a suitable biomaker for liver cancer (R. Zhang et al., 2015) and germ cell tumor (Wu et al., 2015b). The concentration of AFP in normal human serum is less than 25 ng/mL (Chen et al., 2018). The AFP concentration in adult plasma is usually considered an early diagnosis indication of hepatocellular or endodermal sinus tumors. Therefore, the development of a sensitive method for AFP detection in complex biological samples has an important clinic significance. Up to now, several methods have been developed for the determination for AFP, including surface-enhanced Raman scattering (Wu et al., 2015b), electrochemistry (Y. Wang et al., 2015), colorimetry (F. Zhang et al., 2015), and capillary electrophoresis (Funano et al., 2015). However, several limitations are associated with these methods, such as expensive instrumentation and time-consuming operations. Electrochemiluminescence (ECL) technology has been developed rapidly because it provides high sensitivity, low background and a simple design and powerful tool for environmental monitoring (Cheng et al., 2014; Jiang et al., 2015), food safety (Wu et al., 2012), and bioanalysis (Ji et al., 2014; P. Zhang et al., 2015).

Molecularly imprinted polymers (MIPs) are artificial receptors created from templated polymerization. These polymers have excellent properties, such as exhibiting enzyme-like activities or antibody-like binding properties. Due to its stability at harsh conditions, its ease of preparation, and its selective template recognition, MIPs have been widely used in catalysis (Guo et al., 2014), molecular sensing (Xu and Lu, 2015) and separation (Nematollahzadeha et al., 2014).

Molecular imprinting of macro-molecular, particularly proteins, is extremely challenging, due toconformational changes of-templates that take place during polymerization and the difficulty in removing these templates (Chen et al., 2011; Yang et al., 2012). Many approaches have been used for the imprinting of proteins, including epitope imprinting

* Corresponding author.
E-mail address: dengby16@163.com (B. Deng).

https://doi.org/10.1016/j.bios.2018.11.013
Received 15 September 2018; Received in revised form 25 October 2018; Accepted 10 November 2018
Available online 20 November 2018
0956-5663/

(Y. Zhang et al., 2015), surface imprinting (Wang et al., 2014), Pickering emulsion imprinting (Shen et al., 2012), nanotechnology-based imprinting (Cai et al., 2010), microcontact imprinting (Lee et al., 2014), etc. Boronic acids can covalently interact with cis-diol-containing molecules, such as sugars, to generate stable cyclic esters in an alkaline aqueous solution. However, when the environmental pH is shifted to a more acidic pH, the boronate esters dissociate (Li et al., 2013). Boronate affinity molecular imprinting is a novel, simple, and universally applicable method for imprinting glycoproteins. Boronate affinity-based molecular imprinting involves two approaches: photolithographic boronate affinity molecular imprinting (Li et al., 2013) and boronate affinity based oriented surface imprinting (Xing et al., 2017). The boronate affinity molecular imprinting method was significantly different from other imprinting methods. Boronate affinity molecular imprinting is based on the covalent interactions between templates and boronic acids. However, other imprinting methods are based on the non-covalent bonding between functional monomers and templates. The boronate affinity MIP exhibits some excellent peculiarities, such as ease controlling the release/binding (pH < 3 off, pH ≥ 5 on), high affinity, high specificity and outstanding anti-interference (Li et al., 2013). Boronate affinity MIPs are appealing alternatives to antibodies, which have been widely used in immunoassay (Shinde et al., 2015; Wang et al., 2016). Liu's team exploited a series of boronate affinity molecularly imprinted polymers linked to different substrates via oriented surface imprinting, and were used to construct highly sensitive and selective glycoproteins assays the term boronate affinity sandwich assay (BASA) was proposed for the first time (Bi and Liu, 2014; Bie et al., 2015; Ye et al., 2014;). Lin's group prepared boronate-functionalized molecularly imprinted monolithic column for enriching and recognizing glycoproteins (Lin et al., 2013). Ai's team fabricated a highly sensitive glycoprotein biosensor based on a boronate affinity surface that was imprinted using polymers through electrochemical polymerization coupled with nanomaterials for determination of glycoprotein (Wang et al., 2013).

This study combined the merits of surface imprinting and functionalized SiO_2@CQDs/AuNPs to prepare a new ultrasensitive ECL sensor for the analysis of alpha-fetoprotein (AFP). As far as we are aware, the ECL sensor based on boronate affinity-based oriented surface imprinting and functionalized SiO_2@CQDs/AuNPs for AFP detection has not been reported. The principle of the proposed method is shown in Scheme 1. Scheme 1A displays the preparation of the signal amplification tracing label SiO_2@CQDs/AuNPs/MPBA. First, SiO_2@CQDs were prepared through the co-adsorption of self-prepared CQDs and SiO_2. Then, SiO_2@CQDs were modified sequentially via stirring of AuNPs and MPBA, resulting in SiO_2@CQDs/AuNPs/MPBA nanocomposites, which were employed to produce an ECL signal and bind to alpha-fetoprotein, respectively. As illustrated in Scheme 1B, boronate- affinity oriented surface-imprinting electrodes were prepared. First, AuNPs-GO was assembled on the glassy carbon electrode (GCE) using chitosan. Then, MPBA was immobilized on AuNPs-GO via Au-S bonds to capture the target AFP. Next, molecularly imprinted polymer (MIP) film was obtained using methacrylic acid and 4-vinylphenylboronic acid as the functional monomer, ethyl glycol dimethacrylate (EGDMA) as the cross-linker and 2,2′-azobisisobutyronitrile (AIBN) as the initiator. Finally, boronate affinity-based AFP imprinted polymer film was obtained by washing the template AFP. The preparation of the MIP-target-SiO_2@CQDs/AuNPs/MPBA sandwich ECL sensor and the ECL detection process of AFP are displayed in Scheme 1C. Using alpha-fetoprotein (AFP) as a representative target, we evaluated the effects of imprinting conditions and detection conditions. A new multiple signal amplification method was designed based on the SiO_2@CQDs/AuNPs/MPBA sandwich, boronic acid, and molecularly imprinted spatial matched cavities for ultrasensitive ECL detection of alpha-fetoprotein (AFP). This novel boronate-affinity sandwich assay (BASA)-based AFP sensor was successfully applied to determine the concentration of AFP in human serum.

2. Experimental

2.1. Reagents

Graphene oxide (GO) was purchased from Nanjing XFNANO Materials Tech Co., Ltd. (Nanjing, China). Sodium dodecyl sulfate (SDS), bovine serum albumin (BSA), and lipase (LPS) were purchased from Beijing Solarbio Science & Technology Co., Ltd. (Beijing, China). Tetraethylorthosilicate (TEOS), 3-aminopropyltrimethoxysilane (APTMS), 4-vinylphenyboronic acid (VPBA), 2,2′-azobisisobutyronitrile (AIBN), ethyl glycol dimethacrylate (EGDMA), and sodium citrate were purchased from Aldrich (Shanghai, China). $HAuCl_4$ and 4-mercaptophenylboronic acid (MPBA) were purchased from Energy Chemical (Shanghai, China). $NaBH_4$ was purchased from Shanghai Tianlian Fine Chemical Engineering Co., Ltd. (Shanghai, China). Hexane was purchased from Tianjin Fuchen Chemical Reagent Factory (Tianjin, China). Methacrylic acid (MAA) was purchased from Beijing Bailingwei Technology Co., Ltd. (Beijing, China). $K_2S_2O_8$ was purchased from Guangzhou Chemical Reagent Factory (Guangzhou, China). Ethyl alcohol, acetonitrile, ammonium hydroxide, citric acid, NaOH, Na_2HPO_4 and NaH_2PO_4 were purchased from Xilong Chemical Co., Ltd. (Guangdong, China). Alpha-fetoprotein (AFP) and CA153 were purchased from Beijing Biosynthesis Biotechnology Co., Ltd. (Beijing, China). Transferrin (TRF) was purchased from shanghai Yuanye Biotechnology Co., Ltd.(Shanghai, China). The human serum samples were provided by Guilin Fifth people's hospital and stored at 4 °C (Guilin, China). Phosphate buffer solution (PBS, 0.1 mol/L, pH 7.4), prepared by mixing the stock solutions of NaH_2PO_4 and Na_2HPO_4, was used as the supporting electrolyte. Double-distilled water (DDW) was used throughout.

2.2. Apparatus

The ECL responses were carried out on an MPI-B ECL analyzer (Xi'an Remex Electronic Science-Tech Co., Ltd., China) with a voltage of 800 V supplied to the photomultiplier tuber (PMT). An Ag/AgCl (saturated KCl) electrode, a glass carbon electrode (GCE, 3 mm in diameter) and a platinum wire were used as the reference electrode, working electrode and counter electrode, respectively. Surface morphological images and energy-dispersive spectroscopy (EDS) spectra were gained by a model Vario Micro Cube Scanning electron microscopy (SEM) (Elementar Company, Germany). The model SK3310HP ultrasonic cleaner was produced by Shanghai Kudos Ultrasonic Instrument Co., Ltd. (Shanghai, China). Fourier transform infrared spectra (FT-IR) were measured on a PerkinElmer FT-IR spectrophotometer (Perkin-Elmer, USA). Atomic force microscopy (AFM) images were obtained from a Veeco-Multimode-V atomic force microscopy in tapping mode (Veeco, USA). Electrochemical signals were measured on a CHI 660 electrochemical workstation (CH Instruments Co., Shanghai, China).

2.3. Synthesis of tracing tag SiO_2@CQDs/AuNPs/MPBA

Scheme 1A schematically describes the preparation of tracing tag SiO_2@CQDs/AuNPs/MPBA. The syntheses of carbon quantum dots (CQDs), silica/carbon quantum dots (SiO_2@CQDs) (C. Wang et al., 2015), and Au nanoparticles (Au NPs) (Patricia and Ignacio-de, 2013) are prepared according to previous literatures with some modifications. The details were given in the Supplemental Information (S1.1, S1.2 and S1.3). SiO_2@CQDs/AuNPs/MPBA was synthesized via stirring. In a typical synthesis, 45 mL of the AuNPs solution and 5 mL of the 3 mg/mL SiO_2@CQDs homogeneous suspension were uniformly mixed under stirring for 10 h. With the Au nanoparticles began adsorbing onto the surface of SiO_2@CQDs, the light pink color of the solution gradually receded. The products were obtained by centrifuging, washing with water three times and drying in air overnight at 80 °C. The preparation

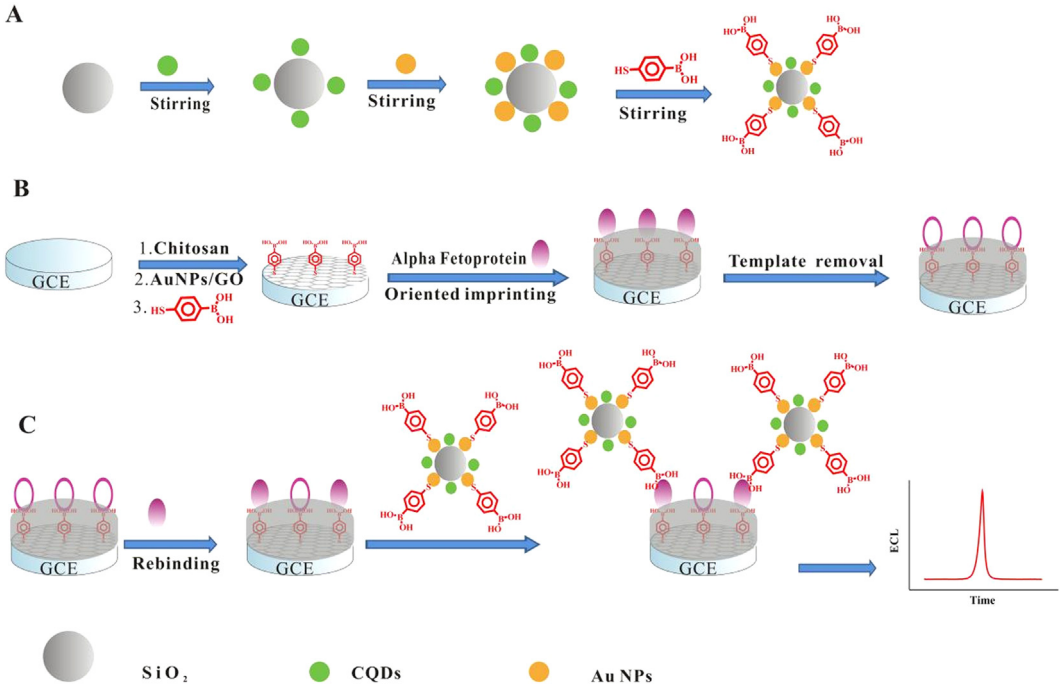

Scheme 1. Schematic fabrication of ECL sensor and ECL detection: (A) preparation of SiO_2@CQDs/Au NPs/MPBA. (B) Preparation process of the boronate affinity based AFP imprinted electrode. (C) Fabrication of the boronate affinity sandwich sensor and the ECL detection of AFP procedure.

of the tracing tag, SiO_2@CQDs/AuNPs/MPBA, consisted of the following steps: 6 mg of the synthesized SiO_2@CQDs/AuNPs was dispersed in 6 mL ethyl alcohol, and an ultrasound was performed on the suspension. Then 2.0 mmol/L MPBA was added with magnetic stirring for 24 h, and under N_2 atmosphere. The final products were centrifuged, washed with aliquots of water, ethanol and hexane and finally dried at 80 °C, to get the light purple tracing tag, SiO_2@CQDs/AuNPs/MPBA.

2.4. Fabrication of the boronate affinity based MIP decorated electrodes

Prior to the construction, the GCE was carefully polished with 0.3 and 0.05 μm alumina slurry to a mirror-like surface. Then the electrode was successively rinsed with ethanol and DDW, and dried under N_2 stream. The AuNPs-GO was prepared according to a previous literature (Wu et al., 2015a) and the detail was provided in the Supplemental information (S1.4). Firstly, the pretreated GCE was decorated by dropping 5 μL of 1% chitosan solution and drying in air. Then 5 μL of the 1.5 mg/mL AuNPs-GO suspension was coated onto its surface and dried in room temperature. After that, the modified electrode was immersed in a 3 mL solution of 100 μmol/L MPBA in ethanol for 12 h. Subsequently, the decorated electrode was rinsed thoroughly with ethyl alcohol and water to remove residual reagents and was dried in room temperature. In order to construct a thin template layer, 5 μL of 0.1 mg/mL AFP solution in phosphate buffer (0.1 mol/L, pH 8.0) was dropped onto the boric acid functionalized electrodes surface and the electrode was then incubated for 30 min, and washed with 0.1 mol/L phosphate buffer solution (pH 8.0). The template coated electrodes were immersed in a 3 mL mixture containing 1.0 mmol/L MAA, 2.0 mmol/L VPBA, 1.25 mmol/L EGDMA and 5.0 mmol/L AIBN for 12 h at room temperature. Ultimately, in order to remove the template, the electrodes were washed with 0.1 mol/L HCl containing 10% SDS (W/V). For comparison, non-imprinted polymer (NIP) coated electrodes were also prepared under the same conditions but without immobilization the template on the boronic acid functionalized electrodes.

2.5. Analysis procedure

A series of 5 μL AFP solutions of different concentrations containing 0.1 mol/L phosphate buffer (pH7.4) were dropped on every MIP decorated electrode, and then incubated for 45 min under humid environment. Subsequently, the MIP decorated electrodes were rinsed with water-acetonitrile solution (7:3, V/V) for 3 min. The rebinding AFP on the MIP decorated electrode was incubated with 5 μL of SiO_2@CQDs/AuNPs/MPBA for 15 min. Finally, the electrodes were slowly rinsed with acetonitrile-phosphate buffer solution (10 mmol/L, pH 9.0) (3:7, V/V) for 3 min, and then dried. The ECL measurements were accomplished with the electrodes in 0.1 mol/L PBS (pH 7.4) containing 0.1 mol/L $K_2S_2O_8$ and scanned between −2.0 V and 0 V with a scan rate of 0.1 V/s. The voltage of the photomultiplier tube (PMT) was set at 800 V.

3. Results and discussion

3.1. Materials characterization

Fig. 1 showed SEM images of SiO_2@CQDs, SiO_2@CQDs/AuNPs/MPBA, MIP loaded AFP on the modified GCE, and MIP after removal of the template AFP on the modified GCE. However, the SEM images of SiO_2 and SiO_2@CQDs/AuNPs were provided in the Supplemental information (Fig. S1A and Fig. S1B). It can be seen that the pure SiO_2 nanoparticles are uniform spherical shapes and smooth surfaces with an average diameter of about 500 nm (Fig. S1A). Fig. 1A illustrated a lot of small sized CQDs distributed on the surface of SiO_2 nanoparticles, suggesting that SiO_2@CQDs had been successfully synthesized. Fig. S1B illustrated that the SiO_2@CQDs/AuNPs displayed more small sized particles coated on the surface of SiO_2@CQDs compared with the SiO_2@CQDs image, demonstrating that the AuNPs were successfully decorated on the surface of SiO_2@CQDs. Compared with the SiO_2@CQDs/AuNPs, we observed that the SiO_2@CQDs/AuNPs/MPBA illustrated relatively blurred edges (Fig. 1B). This demonstrates that MPBA was successfully decorated on the surface of SiO_2@CQDs/AuNPs. As seen from Fig. 1C, AFP was wrapped by MIP membrane. When the

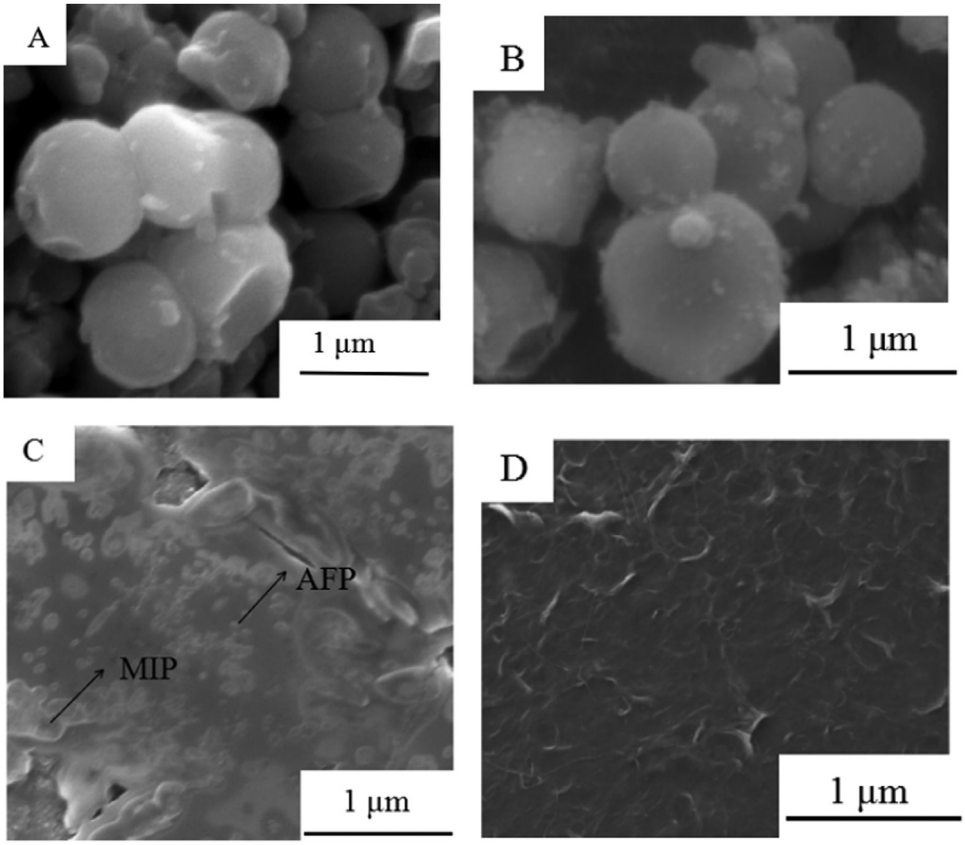

Fig. 1. SEM images ofSiO_2@CQDs (A), SiO_2@CQDs/AuNPs/MPBA (B), MIP loaded AFP on the modified GCE (C), and MIP after removal of the template AFP on the modified GCE (D).

template AFP was washed with 0.1 mol/L HCl containing 10% SDS (w/v) and DDW, the MIP showed many small notches (Fig. 1D). Furthermore, EDS characterization was used for elemental analysis of SiO_2@CQDs/AuNPs/MPBA. As shown in Fig. S1C, the presence of B, C, O, Si and Au elements verified the successful synthesis of SiO_2@CQDs/AuNPs/MPBA. The FT-IR spectra of SiO_2@CQDs (curve a), SiO_2@CQDs/AuNPs (curve b) and SiO_2@CQDs/AuNPs/MPBA (curve c) were used to identify the surface functional groups (Fig. S2A) and the details were given in the Supplemental information (S2.1). In addition, the FT-IR spectra of NIP (curve a), MIP after removal of the template AFP (curve b) and MIP prior washing (curve c) were also measured (Fig. S2B) and the results were explained in the Supplemental information (S2.1).

Atomic force microscope (AFM) was employed to characterize the surface topography of the imprinted layer. The AFM images of NIP membrane and MIP membrane after removing the template are displayed in Fig. 2. The AFM images show a remarkable difference in the roughness of the surfaces, which can be expressed in terms of the root mean square (RMS) value. Moreover, the RMS is proportional to roughness. As illustrated in Fig. 2A, the NIP film was relative smooth and the RMS value was 3.03 nm. However, the MIP film, after removing the template, displayed a rough surface and the RMS value was 11.64 nm (Fig. 2B). The reason for this is because the AFP was successfully deposited in the polymer and then eluted from the film.

The cyclic voltammetry response of different modified electrodes is displayed in Fig. 3A. Firstly, the bare electrode (curve a) emerged a pair of redox peaks of $[Fe(CN)_6]^{3-/4-}$. Secondly, the peak currents were enhanced after decorating the AuNPs-GO on the bare electrode (curve b) based on its superior conductivity. However, the peak current of the MIP decorated AuNPs-GO/GCE sharply decreased (curve c) due to the formation of nonconductive film coated on the surface of AuNPs-GO/GCE and hindered the electron transfer. When the template molecules were eluted from the MIP decorated AuNPs-GO/GCE (curve d), the peak currents increased in comparison to curve c. The loss of AFP can produce imprinting cavities, which increases the diffusion of $[Fe(CN)_6]^{3-/4-}$ through the 3D cavities and the imprinted film. However, the MIP decorated AuNPs-GO/GCE, after rebinding of AFP, displayed much lower peak current compared with curve d, indicating that AFP was rebound on the MIP membrane.

To confirm the successful fabrication of the sensor, electrochemical impedance spectroscopy (EIS) was carried out in a solution containing 5 mmol/L $[Fe(CN)_6]^{3-/4-}$ and 0.1 mol/L KCl, the result of which is displayed in Fig. 3B. Meanwhile the general Randle's equivalent circuit is shown in the inset B1. The electron transfer resistance of the bare GCE was very low with a small semicircle domain (curve a). When modified with AuNPs-GO (AuNPs-GO/GCE, curve b), a smaller semicircle was observed compared with the bare GCE. However, the electron transfer resistance of the MIP modified AuNPs-GO/GCE (curve c) dramatically increased because of electron hindrance of the nonconductive membrane. When the template molecules were removed from the MIP decorated AuNPs-GO/GCE (curve d) the electron transfer resistance decreased relative to curve c. While the AFP was rebounded on the MIP decorated AuNPs-GO/GCE (curve e), the electron transfer resistance increased, which was attributed to the enclosure effect of nonconductive protein molecules during the electron transfer process.

3.2. Optimization of experimental parameters in fabrication of the MIP film

In order to achieve optimal performance for the boric acid affinity imprinted membrane, we optimized the main factors affecting the boric acid affinity imprinting film: the thickness and chemical properties of boric acid imprinted film have an important effect on the activity of the membrane. In this work, we primarily investigated the effect of MPBA and functional monomers MAA and VPBA on boric acid affinity

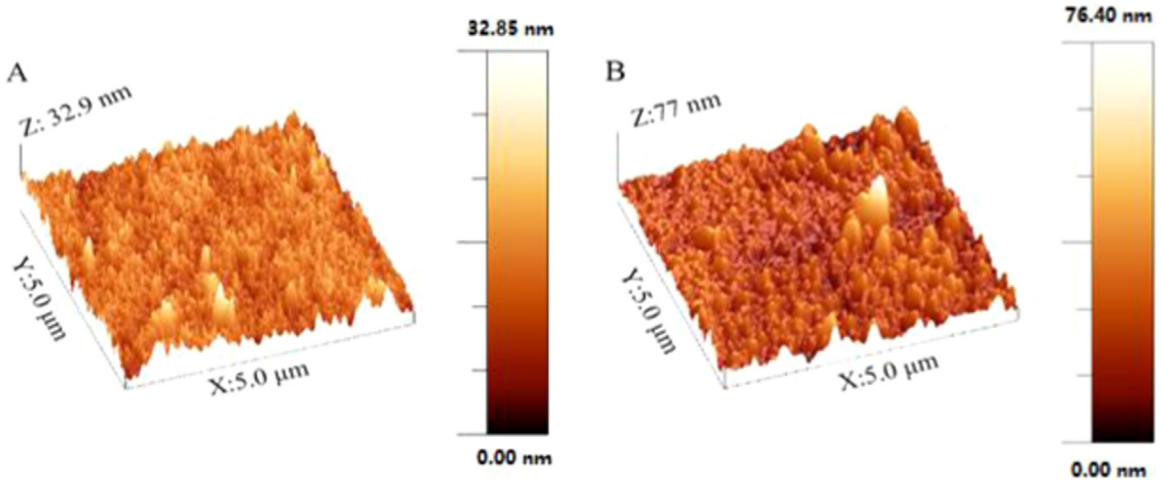

Fig. 2. Atomic force microscopy images of NIP film (A) and MIP film after removing the template (B).

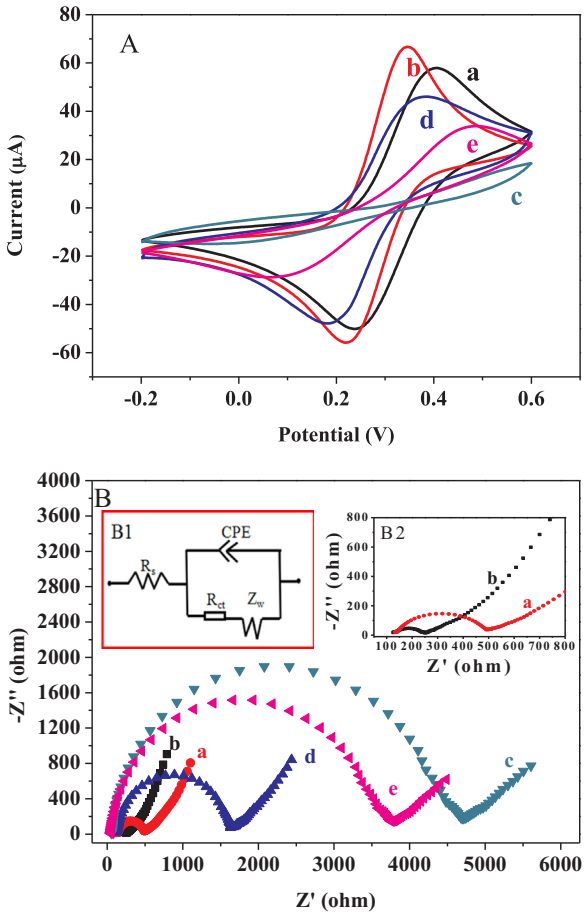

Fig. 3. (A) The CV curves of bare GCE (a), AuNPs-GO/GCE (b), MIP-AuNPs-GO/GCE after molecule imprinting (c), MIP-AuNPs-GO/GCE after removing template molecules (d), MIP-AuNPs-GO/GCE after rebinding of AFP (e). (B) EIS of bare GCE (a), AuNPs-GO/GCE (b), MIP-AuNPs-GO/GCE after molecule imprinting (c), MIP-AuNPs-GO/GCE after removing template molecules (d), MIP-AuNPs-GO/GCE after rebinding of AFP (e). The frequency range is from 0.01 to 100,000 Hz with amplitude of 5 mV. Inset B1: the equivalent circuit applied to fit the impedance data, R_s, solution resistance; CPE, constant phase angle element; R_{et}, electron-transfer resistance; Z_w, Warburg diffusion resistance. Inset B2: magnification of the curves a and b in Fig. 3B. AFP concentration for 10 ng/mL.

imprinted membrane. As shown in Fig. S3A, the absorption of AFP on the MPBA modified electrode surface increased with increase of the concentration of MPBA from 25 to 100 μmol/L. As a result, the ECL intensity gradually increased. However, when the concentration of MPBA exceeded 100 μmol/L, the ECL intensity gradually decreased. This is due to the transfer of excessive amounts of MPBA block electron, which lead to reduction of the ECL signal. The optimal concentration of MPBA was determined to be 100 μmol/L.

In this work, VPBA and MAA were the common functional monomers. There are two reasons for introducing MAA. First, MAA as a common monomer could prominently improve the hydrophilicity of imprinted membrane. Second, the carboxyl group of MAA can be connected with AFP by hydrogen bond to improve the activity of the imprinted film. Therefore, we investigated the effect of molar ratio of MAA to VPBA on the membrane activity. As illustrated in Fig. S3B, when the molar ratio of MAA to VPBA changed from 3:1 to 1:2, the ECL intensity attained maximum value. When the molar ratio was greater than 1:2, the ECL signal gradually reduced. This is due to the concentration of VPBA being too high, which leads to increases in the steric hindrance for binding to AFP. This decrease in binding of imprinted membrane to AFP leads to a decrease in the ECL signal. As a result, the optimal molar ratio of MAA to VPBA was 1:2.

3.3. Optimization of detection condition

In order to obtain the best sensitivity for the sandwich sensor, some important experimental conditions were investigated in detail. The ECL signal of the sandwich sensor was affected by the incubation time of molecularly imprinted membrane modified electrode rebinding AFP. As shown in Fig. S4A, the ECL response increased with increases in incubation time. When the incubation time reached 45 min, the ECL intensity reached a peak. With lengthened incubation time, the ECL intensity basically stays the same. This result suggests saturation of AFP on the sandwich sensor surface. Hence, 45 min was selected as the optimal incubation time. The Fig. S4B was the ECL response of the pH of incubation solution to AFP imprinting on molecularly imprinted electrode. As shown in Fig. S4B, the ECL signal increases as the pH of incubation solution changes from 5 to 8. However, when the pH of the incubation solution is larger than 8, the ECL response gradually decreases. This is because boric acid can react with AFP to form cyclic borate through reversible esterification under weak alkaline conditions.

The pH of buffer solution not only affects the state of substance, but also plays an essential role in the ECL intensity. The effect of PBS pH on the ECL signal was evaluated for the detection cell, with a range between 6 and 8.5. As illustrated in Fig. S4C, there was an increase in ECL response with an increase in the pH. The ECL intensity reaches a

maximum value at a pH of 7.4 because the negative charge accelerates the electron transfer. However, when the pH is higher than 7.4, the excessive negative charge gathered on the electrode surface rejects the $CQDs^{\bullet}$ produced from CQDs obtained electrons, and results in reduction of the ECL intensity. Therefore, pH 7.4 was chosen as the optimal pH of PBS.

In addition, the effect of washing time on the ECL intensity, based on SiO_2@CQDs/AuNPs/MPBA and AFP nonspecific binding, was investigated. As shown in Fig. S4D, the ECL signal gradually decreased with an increase in the washing time. The ECL response reached a stable value when the rinsing time was 3 min. Therefore, 3 min was selected as the optimum washing time.

3.4. ECL behavior of the MIP-target-SiO_2@CQDs/AuNPs/MPBA sandwich sensor

We used AFP as the target protein in order to investigate the performance of BASA. We investigated the ECL behavior of AFP using SiO_2@CQDs/AuNPs/MPBA. After forming the MIP-SiO_2@CQDs/AuNPs/MPBA sandwich with 5 μL of 10 ng/mL AFP, the ECL signals of AuNPs-GO/GCE, NIP-AuNPs-GO/GCE, and MIP-AuNPs-GO/GCE were tested by cyclic voltammetry. The MIP-AuNPs-GO/GCE was incubated with blank AFP containing 0.1 mol/L PBS (pH 7.4) and tested in the same condition. A weak ECL response was observed on AuNPs-GO/GCE (the curve a of Fig. 4A). The ECL signal of NIP-AuNPs-GO/GCE by forming the NIP-target-SiO_2@CQDs/AuNPs/MPBA sandwich was higher than that of AuNPs-GO/GCE (the curve b of Fig. 4A). This was because the polymer decorated electrode surface and MPBA could only adsorbed a small amount of AFP. The ECL signal of MIP-AuNPs-GO/GCE rebinding of AFP was significantly enhanced when the MIP-target-SiO_2@CQDs/AuNPs/MPBA sandwich was absolutely structured (the curve c of Fig. 4A). This result shows that the ECL signal can be amplified by rebinding AFP with SiO_2@CQDs/AuNPs/MPBA based on a molecular imprinting technique. There was a weaker ECL response of MIP-AuNPs-GO/GCE incubated in blank AFP compared with curve a of Fig. 4A (the curve d of Fig. 4A). This result was attributed to cavities of imprinted membrane only adsorbing a small amount of SiO_2@CQDs/AuNPs/MPBA.

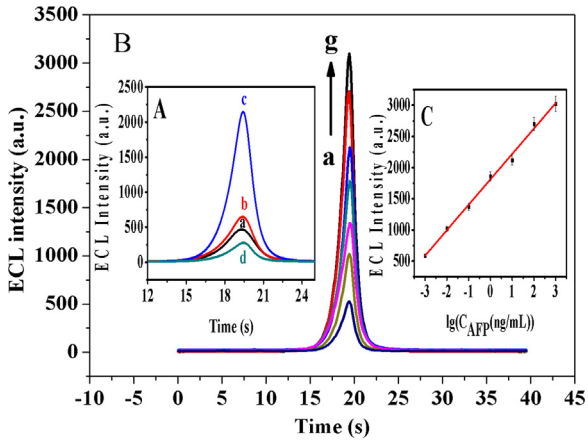

Fig. 4. (A) The ECL responses of AuNPs-GO/GCE (a), NIP-AuNPs-GO/GCE (b), MIP-AuNPs-GO/GCE (c) in 0.1 mol/L PBS (pH 7.4) after incubating in 10 ng/mL AFP solution for 45 min; The MIP-AuNPs-GO/GCE (d) was processed similarly except for incubating in blank AFP-free 0.1 mol/L PBS (pH 7.4). (B) The ECL response of the sandwich sensor for different concentrations of AFP: 0.001 ng/mL (a), 0.01 ng/mL (b), 0.1 ng/mL (c), 1 ng/mL (d), 10 ng/mL (e), 100 ng/mL (f), 1000 ng/mL (g). (C) The plot of the ECL intensity versus the logarithmic of AFP concentration.

3.5. Determination of AFP

We evaluated the concentration dependent response of the sandwich sensor by measuring a series of standard solutions containing different AFP concentrations varied between 0.001 ng/mL and 1000 ng/mL. The ECL response was shown in Fig. 4B. The ECL response gradually increased with increase in the concentration. The limit of detection (LOD) was 0.0004 ng/mL (3σ, n = 11). The linear response varied from 0.001 ng/mL to 1000 ng/mL (Fig. 4C). The linear relation equation was $I_{ECL} = 407.8\log C + 1812$ with a linear relation coefficient of 0.9952. Table S1 compares the analytical performance of the prepared sandwich sensor with other methods (Du et al., 2010; Huang et al., 2013; Lai et al., 2018; Liang et al., 2012; Paramita et al., 2016; Preechakasedkit et al., 2018; Su et al., 2012; Tan et al., 2015). This result demonstrates the merits of our sensor with a lower detection limit and a wider linear range.

3.6. Selectivity, reproducibility and stability of the prepared sandwich sensor

The selectivity of the ECL sandwich sensor was investigated by measuring the ECL response to bovine serum albumin (BSA), lipase (LPS), transferrin (TRF), and CA153 (Fig. 5A). All the interferences observed had responses comparing to the blank sample. However, the ECL signal for AFP showed remarkable increase. These results suggest that the BASA approach has excellent specificity. Fig. 5B shows that the ECL response of the sandwich sensor of 10 ng/mL AFP was tested in 0.1 mol/L PBS (pH7.4) containing 0.1 mol/L $K_2S_2O_8$ for 10 cycles within 400 s. There was no significant decrease on the ECL signal and the relative standard deviation (RSD) was 1.7%. When six consecutive scans of the same sensor were implemented within three days, the interday RSD of ECL intensity was 3.7%. Five sensors of the repeating preparation were measured by the same method, the RSD of ECL signal was 5.4%.

As illustrated in Fig. 5C, the ECL signal of the prepared sensor maintained 94% of the initial signal when the sensor was stored in refrigeration at 4 ℃ for three week, indicating that the proposed sandwich sensor possessed excellent reproducibility and outstanding stability.

3.7. Analysis of AFP in human serum

In order to investigate the applicability of our method in a real sample, we employed the prepared sandwich sensor to measure AFP in human serum samples. The human serum samples were diluted 100 fold using 0.1 mol/L PBS (pH7.4) in order to reduce the nonspecific reaction of albumin and decrease effects of the impedance of albumin on the sensor. The standard addition approach was employed to measure the reliability of the proposed sensor for determination of AFP in human serum. As shown in Table S2, the concentration of AFP in healthy human serum is 13.4 ng/mL. Our recovery percentages ranged from 98.0% to 104% and the RSD ranged from 2.3% to 3.2%, indicating that our proposed method could apply to real sample.

4. Conclusions

This work structured a novel pattern for a boronate affinity sandwich sensor based on SiO_2@CQDs/AuNPs/MPBA, AuNPs-GO and molecularly imprinted membrane cavities to design a multiple signal amplification approach for sensitive ECL determination of AFP in human serum. The affinity of boric acid to glycoprotein AFP and 3D imprinting cavities of molecular imprinted membrane were used to structure the ECL sensor for determination of AFP. This not only improves the sensitivity, but also enhances the selectivity. What's more, when the sandwich sensor was employed to the analysis of AFP in human serum, good recoveries were obtained. The proposed approach is potentially

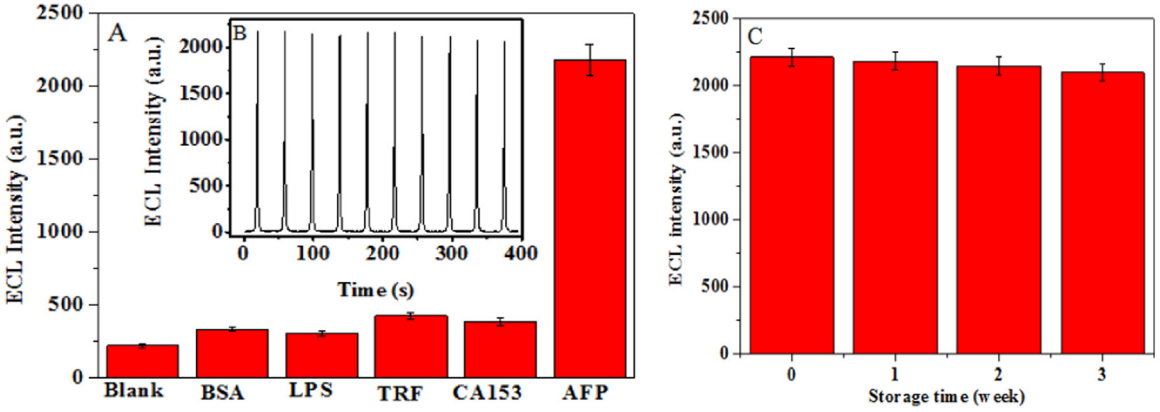

Fig. 5. (A) The ECL intensities were obtained using the sandwich sensor (to blank, 10 ng/mL BSA, 10 ng/mL LPS, 10 ng/mL TRF, 10 ng/mL CA15-3 and 10 ng/mL AFP). (B) Reproducibility of the sensor for incubating 10 ng/mL AFP under consecutive cyclic potential scans 10 times in 0.1 mol/L PBS (pH 7.4) containing 0.1 mol/L $K_2S_2O_8$. (C) Storing stability of the sensor for 0 week, 1 week, 2 weeks and 3 weeks, respectively.

applicable for sensitive determination of AFP for clinical diagnosis.

Acknowledgements

This work was financially supported by the National Natural Science Foundation of China (grant numbers 21765004 and 21365006) and by the Guangxi Science Foundation of China (grant numbers 2014GXNSFDA118004 and 1598025-4), and by the Innovation Project of Guangxi Graduate Education (YCSZ2013039). The research fund of State Key Laboratory for Chemistry and Molecular Engineering of Medicinal Resources (Guangxi Normal University) (CMEMR2017-A5) is gratefully acknowledged. We thank Mr. Jagdeesh Uppal of University of Alberta for editing the English text of the revised manuscript.

Appendix A. Supplementary material

Supplementary data associated with this article can be found in the online version at doi:10.1016/j.bios.2018.11.013.

References

Bi, X., Liu, Z., 2014. Anal. Chem. 86, 12382–12389.
Bie, Z., Chen, Y., Ye, J., Wang, S., Liu, Z., 2015. Angew. Chem. Int. Ed. 54, 10211–10215.
Cai, D., Ren, L., Zhao, H., Xu, C., Zhang, L., Yu, Y., Wang, H., Lan, Y., Roberts, M.F., Chuang, J., Naughton, M.J., Ren, Z., Chiles, T.C., 2010. Nat. Nanotechnol. 5, 597–601.
Chen, F., Zhang, F., Liu, Y., Cai, C., 2018. Talanta 186, 473–480.
Chen, L., Xu, S., Li, J., 2011. Chem. Soc. Rev. 40, 2922–2942.
Cheng, Y., Huang, Y., Lei, J., Zhang, L., Ju, H., 2014. Anal. Chem. 86, 5158–5163.
Du, D., Zou, Z., Shin, Y.S., Wang, J., Wu, H., Engelhard, M.H., Liu, J., Aksay, I.A., Lin, Y., 2010. Anal. Chem. 82, 2989–2995.
Funano, S.I., Sugahara, M., Henares, T.G., Sueyoshi, K., Endo, T., Hisamoto, H., 2015. Analyst 140, 1459–1465.
Guo, Y., Wang, R., Chi, W., Liu, S., Shi, H., Guo, T., 2014. RSC Adv. 4, 7881–7884.
Hart, G.W., Copeland, R.J., 2010. Cell 143, 672–676.
Huang, K., Li, J., Wu, Y., Liu, Y., 2013. Bioelectrochemistry 90, 18–23.
Ji, J., He, L., Shen, Y., Hu, P., Li, X., Jiang, L., Zhang, J., Li, L., Zhu, J., 2014. Anal. Chem. 86, 3284–3290.
Jiang, D., Du, X., Liu, Q., Zhou, L., Qian, J., Wang, K., 2015. ACS Appl. Mater. Interfaces 7, 3093–3100.
Lai, Y., Zhang, C., Deng, Y., Yang, G., Li, S., Tang, C., He, N., 2018. Chin. Chem. Lett. https://doi.org/10.1016/j.cclet.2018.07.011.
Lee, M.H., Thomas, J.L., Lai, M.Y., Shih, C.P., Lin, H., 2014. Langmuir 30, 14014–14020.
Li, L., Lu, Y., Bie, Z., Chen, H., Liu, Z., 2013. Angew. Chem. Int. Ed. 52, 7451–7454.
Liang, R., Wang, Z., Zhang, L., Qiu, J., 2012. Sens. Actuators B 166–167, 569–576.
Lin, Z., Wang, J., Tan, X., Sun, L., Yu, R., Yang, H., 2013. J. Chromatogr. A 1319, 141–147.
Nematollahzadeha, A., Lindemann, P., Sun, W., Stutec, J., Lütkemeyer, D., Sellergren, B., 2014. J. Chromatogr. A 1345, 154–163.
Paramita, K., Ekta, R., Santanu, P., Deepak, K., Rashmi, M., 2016. Biosens. Bioelectron. 78, 454–463.
Patricia, A.A., Ignacio-de, L., 2013. Langmuir 29, 3749–3756.
Preechakasedkit, P., Siangproh, W., Khongchareonporn, N., Ngamrojanavanich, N., Chailapakul, O., 2018. Biosens. Bioelectron. 102, 27–32.
Rudd, R.M., Elliott, T., Cresswell, P., Wilson, I.A., Dwek, R.A., 2001. Science 291, 2370–2376.
Shen, X., Zhou, T., Ye, L., 2012. Chem. Commun. 48, 8198–8200.
Shinde, S., El-Schich, Z., Malakpour, A., Wan, W., Dizeyi, N., Mohammadi, R., Rurack, K., Wingren, A., Sellergren, B., 2015. J. Am. Chem. Soc. 137, 13908–13912.
Su, H., Yuan, R., Chai, Y., Zhuo, Y., 2012. Biosens. Bioelectron. 33, 288–292.
Tan, L., Chen, K., Huang, C., Peng, R., Luo, X., Yang, R., Cheng, Y., Tang, Y., 2015. Microchim. Acta 182, 2615–2622.
Wang, C., Qian, J., Wang, K., Hua, M., Liu, Q., Hao, N., You, T., Huang, X., 2015a. ACS Appl. Mater. Interfaces 7, 26865–26873.
Wang, S., Ye, J., Bie, Z., Liu, Z., 2014. Chem. Sci. 5, 1135–1140.
Wang, S., Yin, D., Wang, W., Shen, X., Zhu, J., Chen, H., Liu, Z., 2016. Sci. Rep. 6, 22757.
Wang, X., Dong, J., Ming, H., Ai, S., 2013. Analyst 138, 1219–1225.
Wang, Y., Wu, D., Zhang, Y., Ren, X., Wang, Y., Ma, H., Wei, Q., 2015b. RSC Adv. 5, 56583–56589.
Wu, B., Wang, Z., Zhao, D., Lu, X., 2012. Talanta 101, 374–381.
Wu, X., Chai, Y., Zhang, P., Yuan, R., 2015a. ACS Appl. Mater. Interfaces 7, 713–720.
Wu, X., Fu, P., Ma, W., Xu, L., Kuang, H., Xu, C., 2015b. RSC Adv. 5, 73395–73398.
Xing, R., Wang, S., Bie, Z., He, H., Liu, Z., 2017. Nat. Protoc. 12, 964–987.
Xu, S., Lu, S., 2015. Chem. Commun. 51, 3200–3203.
Yang, K., Zhang, L., Liang, Z., Zhang, Y., 2012. Anal. Bioanal. Chem. 403, 2173–2183.
Ye, J., Chen, Y., Liu, Z., 2014. Angew. Chem. Int. Ed. 53, 10386–10389.
Zhang, F., Zhu, J., Li, J., Zhao, J., 2015a. J. Mater. Chem. C 3, 6035–6045.
Zhang, P., Wu, X., Yuan, R., Chai, Y., 2015b. Anal. Chem. 87, 3202–3207.
Zhang, R., Pan, B., Wang, H., Dan, J., Hong, C., Li, H., 2015c. RSC Adv. 5, 38176–38182.
Zhang, Y., Deng, C., Liu, S., Wu, J., Chen, Z., Li, C., Lu, W., 2015d. Angew. Chem. Int. Ed. 54, 5157–5160.